Hindawi
Advances in Civil Engineering
Volume 2021, Article ID 8813409, 12 pages
https://doi.org/10.1155/2021/8813409

Research Article

Determination of Joint Surface Roughness Based on 3D Statistical Morphology Characteristic

Hang Lin,[1] **Jianxin Qin**,[1,2] **Yixian Wang**,[3] **and Yifan Chen**[1]

[1]*School of Resources and Safety Engineering, Central South University, Changsha, Hunan 410083, China*
[2]*Power China Zhongnan Engineering Corporation Limited, Changsha, Hunan 410014, China*
[3]*School of Civil and Hydraulic Engineering, Hefei University of Technology, Hefei, Anhui 230009, China*

Correspondence should be addressed to Yifan Chen; 1051361824@qq.com

Received 29 May 2020; Accepted 21 August 2021; Published 6 September 2021

Academic Editor: Paolo Castaldo

Roughness significantly affects the shear behavior of rock joints, which are widely encountered in geotechnical engineering. Since the existing calculation methods on the joint roughness coefficient (JRC) fail to obtain a sufficiently accurate value of JRC, a new determination method was proposed in this study, where the 3D laser scanning technique and self-compiled Python code, as well as the statistical parameter methods, were applied. Then, the shear strength of jointed rock was evaluated via Barton's model, and therefore, a comprehensive comparison between the calculating results and experimental results was executed. Ultimately, the influencing factors of roughness profile extraction on the accuracy of JRC value, such as the measuring point interval, profile number, and measuring direction, were investigated. The results show that (1) equipped with the 3D laser scanning technique, the roughness profiles can be accurately extracted via the self-compiled Python code, (2) an excellent consistency of shear strength could be observed between the calculating value and experimental results, verifying the validity and accuracy of the proposed method, and (3) a smaller measuring point interval can produce a more accurate digital profile and more accurate JRC value. To a certain extent, the more the sample numbers of profiles, the smaller the value of JRC.

1. Introduction

Rock joints widely exist in rock engineering [1–4]. The mechanical properties of rock joints are considered as the controlling factors of rock mass engineering stability [5–8]. Previous research studies have shown that the roughness remarkably affects the friction angle, shear expansion, and peak shear strength of jointed rock mass [9–13]. By considering the roughness of joint (JRC) and presenting 10 standard joint contour curves, Barton and Choubey [14] established the JRC-JCS shear strength model, which is popular in evaluating rock mass stability in geotechnical engineering. Despite empowering a significant efficacy in the shear strength calculation of jointed rock mass, it incurs some controversies with respect to the quantification to the joint roughness, promoting a wide pursue of the determination method of JRC in recent years [15–17]. For example, Tse et al. [15] studied the relationship between 11 joint parameters and JRC value. Gadelmawla et al. [18] enumerated 59 parameters describing joint surface morphology. Li et al. [19] normalized the symbols of many joint parameters and optimized the calculation formula between these parameters and the JRC. Some other scholars [20–22] introduced the fractal theory into rock mechanics to evaluate the JRC and achieved expectant results.

The measurement to the joint surface relief morphometry is usually executed via the needle profile comb [23–25], which neglects the fluctuation characteristics smaller than the measuring interval and extra terraced characteristics to the original profile [26]. Experimental evidences [27] showed that the difference of the JRC is up to 4 when the error of fluctuation measurement is 1 mm. In this case, some other optional methods, such as statistical parameter, straight edge, elongation, and geometric fractal methods, have been developed to quantitatively determine the value of JRC [16, 17, 28–30]. However, the straight edge

method can only consider the large fluctuations of the joint, the elongation method totally ignores the influence of fluctuations, and the roughness described by fractal theory significantly varies for different joint samples. Based on strict mathematical calculation, the statistical parameter method shares a sufficient accuracy on the measurement to the joint surface relief morphometry, which can avoid the error caused by subjective factors and is convenient to calculate the value of JRC. Almost all the statistical parameter methods are only used for the description of JRC in 2D, which may result in distortion in practical application. Due to the limitation of the amount of information, the parameter values have large deviations and limitations. Therefore, 3D JRC profiles must be developed to account for the variation of roughness profiles in 3D space [31].

In this study, a new method based on the 3D scanning technique and Python code was presented to accurately describe the roughness of joints. Particularly, the joint surface was divided into several rectangular regions. For each region, the 3D scanning technique was applied to obtain the 3D coordinate data, the Python code was used to extract the roughness profile, and the value of JRC was calculated via the statistical parameter methods, where Z_2 (the first derivative root mean square of roughness profiles), structure function (SF, representing the changes in surface texture), and R_p (the length ratio of the trace line to the straight line) were selected. Then, the arithmetic average of JRC of all regions was solved to represent the roughness of the joint surface, denoted as JRC_p, which avoids the subjective estimation. To obtain accurate JRC values, the shear direction is also considered [32]. In addition, the calculated JRC_p is embedded in the current shear strength formula of joint, and the calculating results by the proposed JRC_p determination method present a significant consistency with the test results, which verified the validity and accuracy of the proposed method. Finally, the influencing factors of roughness profile extraction on the accuracy of JRC_p, such as the measuring point interval, profile number, and measuring direction, were investigated.

2. Joint Surface Morphology Acquisition

2.1. Preparation of Samples. Four mortar samples (100 mm × 100 mm × 100 mm in size) with 45° sawtooth were prepared, and the failure surfaces by direct shear test under four different normal stresses were, therefore, selected as the research objects (see Figure 1). For convenience, the failure surface was numbered by its normal stress, at the ascending order, which corresponds to sample No. 1~4. The samples were produced according to the proportion of white cement : fine sand : water = 1.5 : 1.5 : 0.8 and maintained under standard conditions for 28 days. After the specimens are cured, the Brazilian split test and uniaxial compression test can be performed. The size of the sample used in the Brazilian splitting test is a cylinder of 25 mm × 50 mm (height × diameter), and the surface flatness of the test sample is in the range of 0.02 mm. The cylindrical end portion is perpendicular to the axis of the specimen, with a tolerance of ±0.25°. Before the test begins, the steel rod needs to be glued on both the sides of the cylindrical end portion to conduct compressive stress. During the test, the load was loaded at a small displacement of 0.5 mm/min. When the sample in the radial tensile failure, the tensile strength of the material can be obtained according to experimental data recording and experimental curves. The size of the sample used in the uniaxial compressive strength test is a cylinder of 100 mm × 50 mm (height × diameter), the sample has the same tolerance as the Brazilian cracked disk test [33, 34], and the compression load is 400 N/S. The uniaxial compressive strength of the sample is 18.97 MPa, and the tensile strength measured by the Brazilian splitting test is 1.64 MPa. Direct shear tests were conducted at the normal stresses of 0.8 MPa, 1.2 MPa, 1.6 MPa, and 2.0 MPa, respectively. The shear box size is 100 mm × 100 mm × 100 mm, and the shear strain rate is 1 mm/min in the direct shear test.

2.2. Test Apparatus. The apparatus used in this study is HL-3DC color 3D scanner, which is mainly composed of computer, control unit, laser scanning device, and data acquisition software. The laser scanning device is the core of the apparatus, which consists of a central projection unit sensor head and two charge-coupled device (CCD) cameras. During the scanner operation, the central projection unit projects a series of continuous grating stripes with different widths on the joint surface, and the two CCD cameras record the related scanning information from two different angles and integrate them into the measuring head to determine the coordinate data on the surface of the object (see Figure 1). The details of the surface can be captured by laser measurements due to the introduction of high data density. Briefly, the scanner shares high scanning speed and remarkable scanning accuracy.

2.3. Procedures to Extract Roughness Profiles. The procedures for the roughness profiles extraction of the failure surfaces are expressed in detail as follows:

(1) Affixing marking points on the failure surface: the target surface should be divided into parts and scanned because the laser projected by a 3D laser scanner cannot cover the entire failure surface at the once time. The marked points must be affixed on the failure surface to accurately splice the scanned data of each part (see Figure 1(a)).

(2) Scanning failure surface: next, the failure surface is scanned on the scanning platform, which is rotated or moved after each scan to ensure that the entire failure surface has been scanned (see Figure 1(b)).

(3) Point cloud processing: the built-in software automatically splices the scanning data to obtain the point cloud data of the entire surface based on the marking points (see Figure 1(c)).

(4) Digital modeling of the failure surface: the point cloud data are processed to obtain the digital model of the failure surface, and the 3D coordinates of each scanning point can be outputted based on the required precision (see Figure 1(d)).

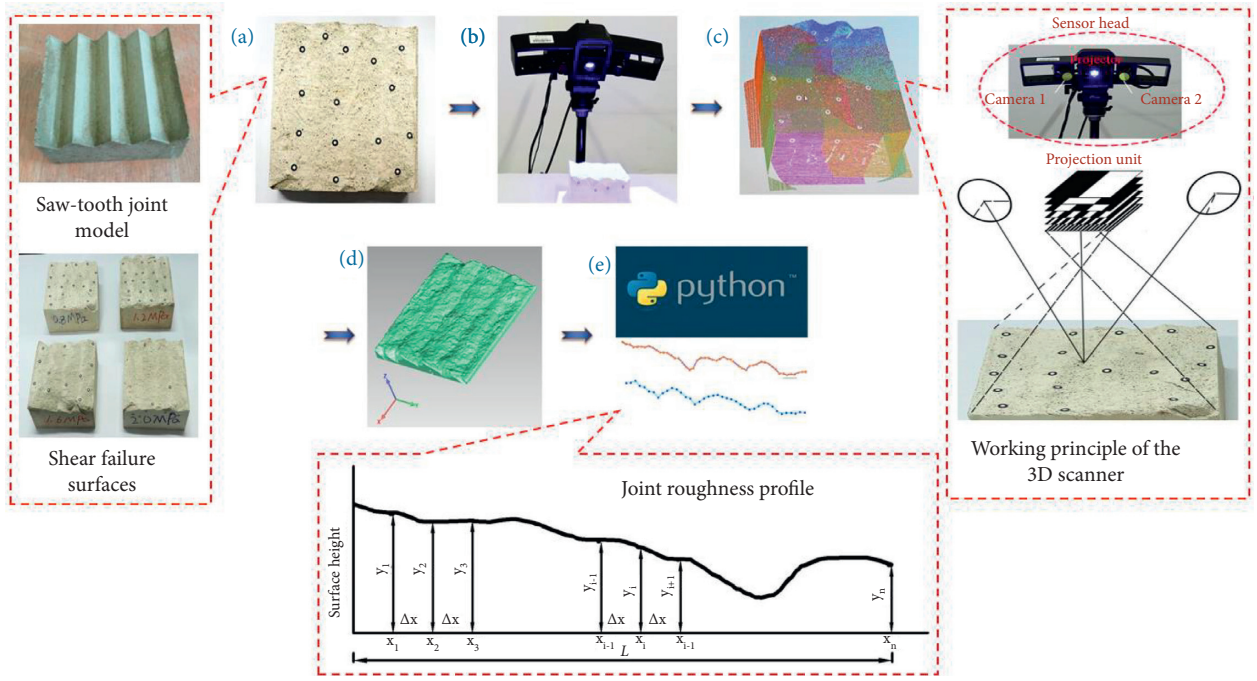

Figure 1: The extraction process of the sawtooth joint roughness profile.

(5) Extracting the roughness profiles of the failure Surface: processing the 3D coordinates based on the self-compiled Python code, the roughness profiles of the failure surface can be extracted (see Figure 1(e)).

3. Determination of Surface Roughness

3.1. Description of Statistical Parameters for Roughness Profiles. In previous research studies, there have been numerous statistical parameters, such as the root mean square of the surface height of joint, the average of the center line, average roughness, the average roughness angle, and the standard deviation of the roughness angle, proposed to describe the roughness characteristics of the shear surface [35–37]. However, in this study, the roughness was characterized by statistical parameters Z_2, SF, and R_p. Specifically, Z_2 is the mean square root of the first derivative of profile, as shown in equation (1), which is widely used in surface roughness analysis and is first proposed to measure the light scattering property of the metal surface [15]. The structure function (SF) is used to represent the changes in surface textures, which can be calculated using equation (2). In addition, El-Soudani [38] proposed that the ratio of trace length to straight line length (R_p) can be used to represent the linear roughness of object surface, as shown in equation (3). The larger the value of R_p is, the rougher the profile will be. Due to the constant relationship of $R_p \geq 1$, $R_p - 1$ is usually adopted for research convenience.

$$Z_2 = \left[\frac{1}{L}\int_{x=0}^{x=L}\left(\frac{\mathrm{d}y}{\mathrm{d}x}\right)^2 \mathrm{d}x\right]^{1/2} = \left[\frac{1}{L}\sum_{i=1}^{n-1}\frac{(y_{i+1}-y_i)^2}{(x_{i+1}-x_i)}\right]^{1/2}, \tag{1}$$

$$\mathrm{SF} = \frac{1}{L}\int_{X=0}^{x=L}[f(x+\mathrm{d}x)-f(x)]^2\mathrm{d}x = \frac{1}{L}\sum_{i=1}^{n-1}(y_{i+1}-y_i)^2(x_{i+1}-x_i), \tag{2}$$

$$R_p = \frac{\sum_{i=1}^{n-1}\left[(x_{i+1}-x_i)^2+(y_{i+1}-y_i)^2\right]^{1/2}}{L}. \tag{3}$$

The roughness profile is shown in Figure 1. x_i represents the horizontal coordinates along the profile, y_i represents the vertical coordinates corresponding to x_i on the profile, L represents the horizontal length of the profile, and n is the total number of measuring points of the profile. The statistical parameters of Z_2, SF, and $R_p - 1$ corresponding to each profile extracted can be calculated according to equations (1)–(3). Jang and Kang [39] studied 10 standard JRC curves of Barton by using an accurate digitization technique and obtained the relationship between the statistical parameters Z_2, SF, $R_p - 1$, and JRC of joints, which are expressed as follows:

$$\mathrm{JRC} = 51.16\left(Z_2\right)^{0.531} - 11.44, \tag{4}$$

$$\mathrm{JRC} = 73.95\left(\mathrm{SF}\right)^{0.266} - 11.38, \tag{5}$$

$$\mathrm{JRC} = 65.9\left(R_p - 1\right)^{0.531} - 9.65. \tag{6}$$

To obtain joint surface roughness, several profiles were taken along a certain direction of the joint, dividing the joint surface into several rectangular regions (see Figure 2). Δx is the interval between the two profiles. Profiles AB and CD are infinitely close to each other when Δx is sufficiently small, in which case the roughness of AB and CD can be considered approximate. Thus, the roughness of the rectangular region ABCD can be represented by the average roughness of profiles AB and CD. Similarly, the arithmetic average of the roughness of all the rectangular regions can be assumed as the roughness of the entire joint surface. The surface roughness of the joint obtained by the proposed method is denoted as JRC_p, m is the number of rectangular regions, and the calculation method is shown as follows:

$$\begin{aligned}
\mathrm{JRC}_p\left(Z_2\right) &= \frac{1}{m}\sum_{i=1}^{m}\mathrm{JRC}_p\left(Z_{2i}\right),\\
\mathrm{JRC}_p\left(\mathrm{SF}\right) &= \frac{1}{m}\sum_{i=1}^{m}\mathrm{JRC}_p\left(\mathrm{SF}_i\right),\\
\mathrm{JRC}_p\left(R_p - 1\right) &= \frac{1}{m}\sum_{i=1}^{m}\mathrm{JRC}_p\left(R_p - 1\right)_i.
\end{aligned} \tag{7}$$

3.2. Shear Strength of the Joint Based on JRC_p. To verify the validity and accuracy of the proposed method, the calculated JRC_p is embedded into Barton's shear formula to calculate the shear strength of the joints, as shown in equation (8), and the comprehensive comparison of shear strength between the calculating results and the test results was carried out in this study.

$$\tau = \sigma_n \cdot \tan\left[\mathrm{JRC}_p \times \left(\frac{\mathrm{JCS}}{\sigma_n}\right) + \varphi_b\right], \tag{8}$$

where τ is the peak shear strength of the joint, σ_n is the normal stress, JRC_p is the roughness coefficient of the joint parallel to the shear direction, and JCS is the uniaxial compressive strength of the joint. For the unweathered shear surface, JCS can be represented by the uniaxial compressive strength, which is 18.97 MPa as previously described. The method proposed by Xia and Sun [40] was adopted to obtain the basic friction angle of rock via direct shear tests of flat joint. The shear stress-shear displacement curves of flat joints under different normal stresses are shown in Figure 3.

Note that slight cohesion emerges on the shear surface since the upper blocks were directly cast on the lower blocks when producing the samples, resulting in the occurrences of the peak in shear stress-shear displacement curves. Consequently, the shear strength after stabilization was selected to calculate the basic friction angle. The relationship between

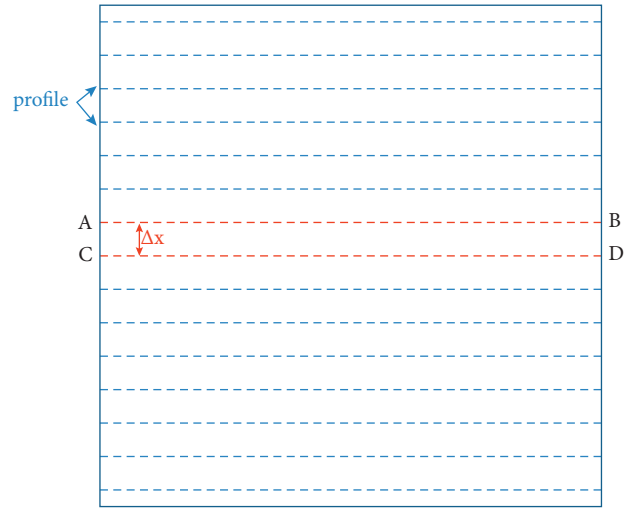

Figure 2: Schematic of determining surface roughness.

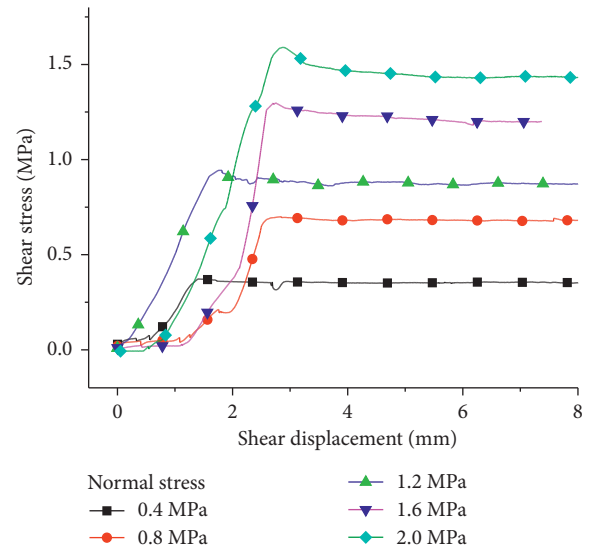

Figure 3: Relationship between shear stress and shear displacement of flat joint.

normal stress and shear strength was fitted in Figure 4, which indicates a basic friction angle of 33.82°, underpinned by the Mohr–Coulomb criterion [41, 42]. Afterwards, the theoretical shear strengths of joints were calculated with equation (8), as shown in Table 1.

Previous research studies show that the shear strength obtained by the secondary shear test of the joint basically approximates to the residual strength of the first shear test under the same loading condition [43]. Thus, in this study, the residual strength of the first shear test was considered equivalent to the shear strength of the secondary shear test. The shear stress-shear displacement curves are shown in Figure 5. The relative error of shear strength was selected to evaluate the feasibility of the proposed JRC_p, which can be calculated as follows:

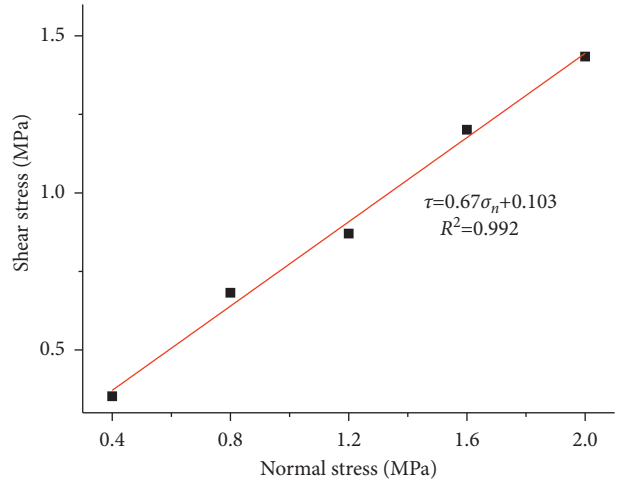

Figure 4: Relationship between shear stress and normal stress.

Table 1: Calculating results and test results of the shear strength.

Specimen number	Type of JRC_p	JRC_p	Calculated result of shear strength	Test result of shear strength	Relative error (%)
1	JRC_p (Z_2)	18.85	1.37	1.20	14.49
	JRC_p (SF)	19.13	1.39		16.29
	JRC_p ($R_p - 1$)	18.05	1.31		9.56
2	JRC_p (Z_2)	17.48	1.70	1.43	18.71
	JRC_p (SF)	17.67	1.71		19.74
	JRC_p ($R_p - 1$)	16.51	1.63		13.74
3	JRC_p (Z_2)	16.81	2.04	1.78	14.56
	JRC_p (SF)	17.86	2.12		19.35
	JRC_p ($R_p - 1$)	15.19	1.92		7.68
4	JRC_p (Z_2)	15.85	2.33	2.14	8.84
	JRC_p (SF)	16.12	2.35		9.87
	JRC_p ($R_p - 1$)	14.97	2.26		5.60

$$\varepsilon = \left| \frac{\tau_{cal} - \tau_{test}}{\tau_{test}} \right| \times 100\%. \quad (9)$$

The shear strength calculated by equation (8) was compared with the test shear strength, as shown in Table 1. The smaller the relative error is, the closer the calculated value to the test value will be. It is evident in Table 1 that the shear strengths calculated by JRC_p agree well with the test results, which proves that the proposed method is reliable in determining the surface roughness of joint. For clarity, the test results and calculating results are plotted in Figure 6 to intuitively assess their consistency, and there exist few differences between the calculating results and the test results, especially for the shear strength calculated by the roughness statistical parameter $R_p - 1$. Therefore, the determination method of joint roughness by $R_p - 1$ was suggested.

3.3. The Influencing Factors of Roughness Profile Extraction. The previously described strategy of roughness determination in this study indicates that the real challenge to obtain an accurate value of the JRC of joint emerges as extracting appropriate roughness profiles, which is quite susceptible by subjective factors. As a result, the influencing factors of the measuring point interval and profile number, as well as profile extraction direction, were further investigated.

3.4. Effect of Measuring Point Interval on Profile Roughness. To investigate the effect of measuring point interval on the profile roughness, one profile was digitized by Python code at the measuring point intervals of 0.5 mm, 1.5 mm, and 2.5 mm, respectively (see Figure 7). Obviously, similar shapes and general fluctuation trend of digital profiles obtained at different measuring point intervals can be observed. With the increase of the measuring point interval, however, the number of measuring points decreases and local details of profiles are easily ignored, accompanied with distortion of digitized profiles. Specifically, the digital description of the profile with highest precision emerges when the measuring point interval is 0.5 mm, while the digital profile of 1.5 mm measuring point interval is distorted. Part local details can no longer be captured at the measuring point interval of 2.5 mm. In contrast, the digital profile with a greater measuring point interval is smoother than that with a smaller measuring point interval. Despite the morphology of the shear surface can be reflected when using the

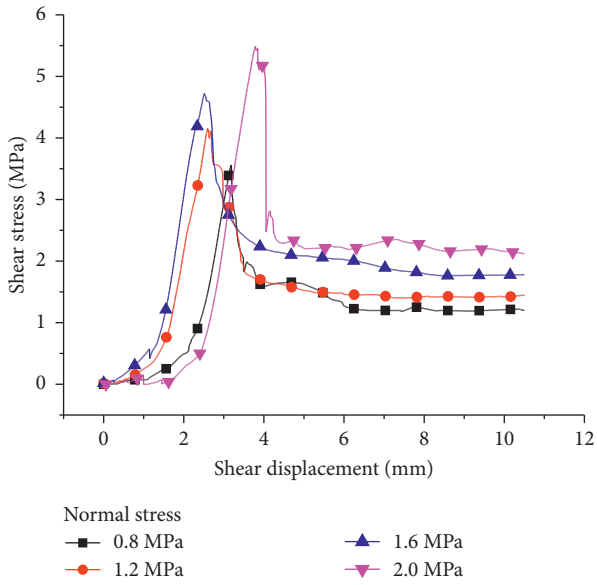

Figure 5: Shear stress-shear displacement of sawtooth joints.

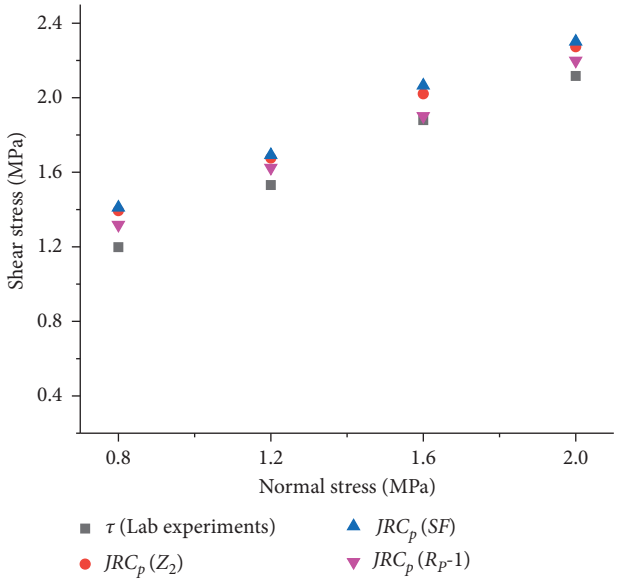

Figure 6: Comparison of shear stress test results and calculating results.

measuring point intervals of 0.5 mm, 1.5 mm, and 2.5 mm to the profile, theoretically a smaller interval can produce a more accurate joint shear surface. Therefore, it is suggested to adopt the measuring point interval as small as possible when extracting the profile.

3.5. Effect of the Profile Number on Statistical Parameters and JRC_p. As previously described, the joint surface was divided into several rectangular regions by profiles, and the joint roughness was represented by the arithmetic average of the roughness of those regions. In this case, whether the number of profiles affects the determination of joint roughness should be investigated. The shear surface of No. 4 sample,

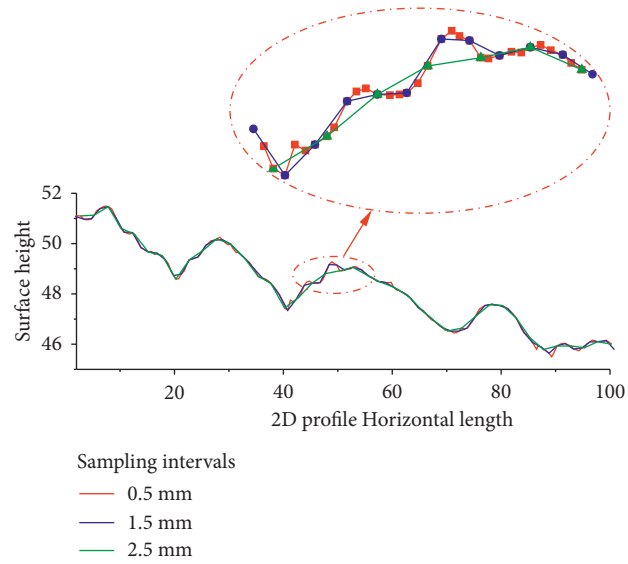

Figure 7: Digital profile with different sampling intervals.

that is, the surface obtained via the shear test under the normal stress of 2.0 MPa, was selected to be the research object, and different numbers of profiles in the shearing direction were extracted, as shown in Figure 8, for the investigation of the influence of the profile number on statistical parameters and JRC_p. The number of profiles in this study was set as 4, 6, 8, 10, and 12. The corresponding statistical parameters and JRC_p are shown in Table 2.

The arithmetic averages of statistical parameters Z_2, SF, and $R_p - 1$ in Table 2 were calculated, respectively. The relationships between statistical parameters and the number of profiles are plotted in Figure 9. Distinctly, the average values of Z_2, SF, and $R_p - 1$ share a similar trend of decrease with the increase of profile number from 4 to 12. Therein, a greater decreasing rate of Z_2 and SF can be observed compared to that of R_p when the profile number increases from 4 to 8, which are slowing down after that. However, the turning point in decreasing rate of R_p is found to be located in the profile number of 10. According to the above phenomenon, to avoid the overestimate of the roughness parameters of joint surface and unnecessary workload, 10–12 profiles are considered appropriate.

Figure 10 describes the variation trends of JRC_p (Z_2), JRC_p (SF), and JRC_p $(R_p - 1)$ when the profiles increase from 4 to 12. JRC_p (Z_2), JRC_p (SF), and JRC_p $(R_p - 1)$ are basically similar for the same profile number, especially for JRC_p (Z_2) and JRC_p (SF), showing a decreasing trend with the increase of the number of profiles. Thus, the conclusion that JRC_p decreases at a slowing rate with the increase of the profile number can be deduced. Note that the value of JRC_p becomes stable when the number of profiles reaches 10. Combining with the analysis of the influence of profile number on the statistical parameters, 10 profiles of shear surface are suggested for JRC calculation.

3.6. Determination of JRC_p in Parallel and Vertical Shearing Directions. The profiles were extracted with an isometric distance parallel to the shearing direction (y direction) and

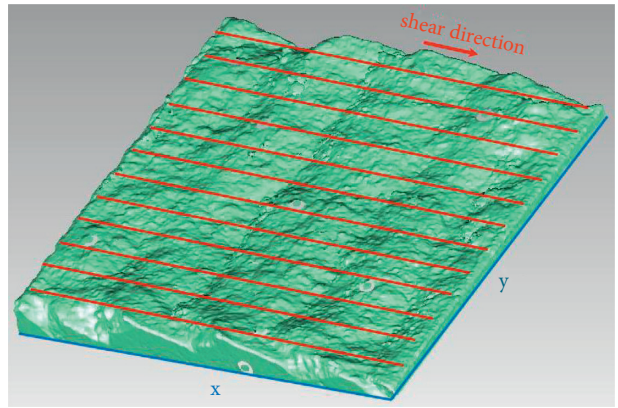

Figure 8: Schematic of profile extraction.

Table 2: Influence of the profile number on statistical parameters and JRC_p.

Number of profiles	Profile number	Z_2	SF	$R_p - 1$	JRC (Z_2)	JRC (SF)	JRC ($R_p - 1$)
4	1	0.334113	0.027908	1.041132	17.14367	17.16313	15.49015
	2	0.323575	0.026175	1.037607	16.66137	16.68062	14.81893
	3	0.336752	0.028351	1.039223	17.26334	17.28285	15.13186
	4	0.516084	0.066586	1.080583	24.56686	24.59143	21.15147
6	1	0.334113	0.027908	1.041132	17.14367	17.16313	15.49015
	2	0.271739	0.018461	1.029877	14.17328	14.19167	13.17641
	3	0.324212	0.026278	1.036949	16.69073	16.70999	14.68901
	4	0.365211	0.033345	1.052989	18.52686	18.54702	17.4888
	5	0.28327	0.020061	1.031734	14.74481	14.76335	13.59582
	6	0.516084	0.066586	1.080583	24.56686	24.59143	21.15147
8	1	0.334113	0.027908	1.041132	17.14367	17.16313	15.49015
	2	0.280668	0.019694	1.031494	14.61681	14.63532	13.54263
	3	0.332411	0.027624	1.042903	17.06624	17.08566	15.81223
	4	0.28135	0.019789	1.02947	14.6504	14.66892	13.08202
	5	0.317278	0.025166	1.038411	16.36962	16.38874	14.97589
	6	0.252274	0.015911	1.025084	13.18208	13.20025	12.0022
	7	0.391934	0.038403	1.055081	19.67193	19.69276	17.80791
	8	0.391647	0.038347	1.06269	19.65981	19.68063	18.90214
10	1	0.334113	0.027908	1.041132	17.14367	17.16313	15.49015
	2	0.308664	0.023818	1.036554	15.96614	15.9851	14.61013
	3	0.291631	0.021262	1.034531	15.15236	15.17103	14.19644
	4	0.323575	0.026175	1.037607	16.66137	16.68062	14.81893
	5	0.29824	0.022237	1.033366	15.47072	15.4895	13.95051
	6	0.348908	0.030434	1.044766	17.80894	17.82872	16.14123
	7	0.336752	0.028351	1.039223	17.26334	17.28285	15.13186
	8	0.272945	0.018625	1.02944	14.23358	14.25198	13.07505
	9	0.286452	0.020514	1.032467	14.90056	14.91915	13.75682
	10	0.368939	0.034029	1.044936	18.6889	18.70915	16.17077
12	1	0.28874	0.020843	1.031503	15.01205	15.03068	13.54462
	2	0.311391	0.024241	1.038002	16.09442	16.11343	14.89633
	3	0.269838	0.018203	1.028985	14.07799	14.09635	12.96833
	4	0.306261	0.023449	1.037605	15.85262	15.87154	14.81867
	5	0.32068	0.025709	1.040139	16.52758	16.54676	15.30524
	6	0.289813	0.020998	1.033059	15.06423	15.08287	13.88487
	7	0.345613	0.029862	1.046337	17.66194	17.68165	16.41125
	8	0.330448	0.027299	1.043801	16.97674	16.99612	15.97202
	9	0.252274	0.015911	1.025084	13.18208	13.20025	12.0022
	10	0.255891	0.01637	1.025643	13.36889	13.3871	12.14687
	11	0.321166	0.025787	1.04031	16.55005	16.56925	15.33727
	12	0.370488	0.034315	1.048407	18.756	18.77628	16.75744

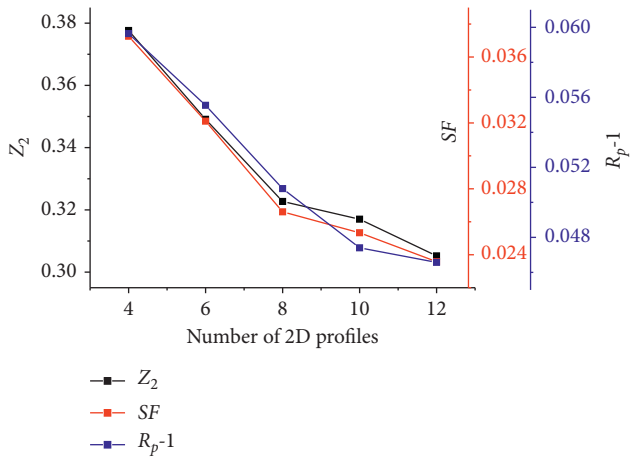

Figure 9: Relationship between statistical parameters and the number of profiles.

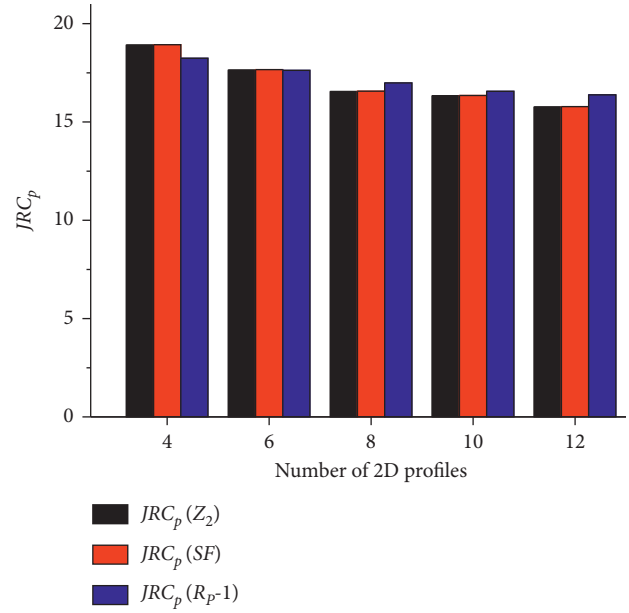

Figure 10: Relationship between JRC_p and the number of profiles.

Table 3: Influence of extraction direction of profile on statistical parameters.

Shear surface	Profile number	Z_2 (x)	SF (x)	R_p (x)	Z_2 (y)	SF (y)	R_p (y)
1	1	0.343042	0.029419	1.051248	0.334809	0.028024	1.044827
	2	0.261163	0.017052	1.032576	0.350642	0.030737	1.045732
	3	0.35155	0.030897	1.054283	0.298106	0.022217	1.040015
	4	0.373058	0.034793	1.061177	0.333896	0.027872	1.042271
	5	0.3997367	0.039947	1.064871	0.342821	0.029382	1.055555
	6	0.377267	0.035583	1.056107	0.4576	0.052349	1.060914
	7	0.412579	0.042555	1.055478	0.525343	0.068996	1.102716
	8	0.362058	0.032772	1.052836	0.30805	0.023724	1.040881
	9	0.390099	0.038044	1.058005	0.404181	0.040841	1.070758
	10	0.443775	0.047938	1.073249	0.372061	0.034607	1.063165

Table 3: Continued.

Shear surface	Profile number	Z_2 (x)	SF (x)	R_p (x)	Z_2 (y)	SF (y)	R_p (y)
2	1	0.358044	0.032049	1.033353	0.381981	0.036477	1.056747
	2	0.263427	0.017348	1.032434	0.380664	0.036226	1.059583
	3	0.290132	0.021044	1.037588	0.392407	0.038496	1.056243
	4	0.320936	0.02575	1.046633	0.373906	0.0349515	1.054571
	5	0.312349	0.024391	1.044121	0.377599	0.035645	1.058774
	6	0.305883	0.023391	1.040688	0.366126	0.033512	1.055402
	7	0.282649	0.019973	1.037073	0.283334	0.020069	1.03763
	8	0.290506	0.021098	1.03886	0.330059	0.027235	1.033379
	9	0.353121	0.031174	1.0543	0.299368	0.022405	1.036668
	10	0.453598	0.051438	1.08151	0.229659	0.013186	1.020064
3	1	0.334113	0.027908	1.041132	0.224982	0.012654	1.024422
	2	0.308664	0.023818	1.036554	0.24325	0.014793	1.028303
	3	0.291631	0.021262	1.034531	0.361477	0.032666	1.040065
	4	0.323575	0.026175	1.037607	0.66201	0.109564	1.075167
	5	0.29824	0.022237	1.033366	0.336357	0.028284	1.051063
	6	0.348908	0.030434	1.044766	0.236292	0.013958	1.024576
	7	0.336752	0.028351	1.039223	0.249817	0.015602	1.029733
	8	0.272945	0.018625	1.02944	0.238031	0.014165	1.026865
	9	0.286452	0.020514	1.032467	0.350299	0.030677	1.04701
	10	0.368939	0.034029	1.044936	0.365196	0.033342	1.048151
4	1	0.457593	0.052348	1.07205	0.221649	0.012282	1.022363
	2	0.296956	0.022046	1.03302	0.251538	0.015818	1.029965
	3	0.240434	0.014452	1.022398	0.336627	0.028329	1.044274
	4	0.231826	0.013436	1.020668	0.374093	0.034986	1.053469
	5	0.268352	0.018003	1.028363	0.386686	0.037382	1.04766
	6	0.230802	0.013317	1.020365	0.361977	0.032757	1.042685
	7	0.192003	0.009216	1.012592	0.326857	0.026709	1.048839
	8	0.261574	0.017105	1.026244	0.275096	0.018919	1.03532
	9	0.330512	0.027309	1.044239	0.302523	0.02288	1.041375
	10	0.278776	0.019429	1.031265	0.224518	0.012602	1.017939

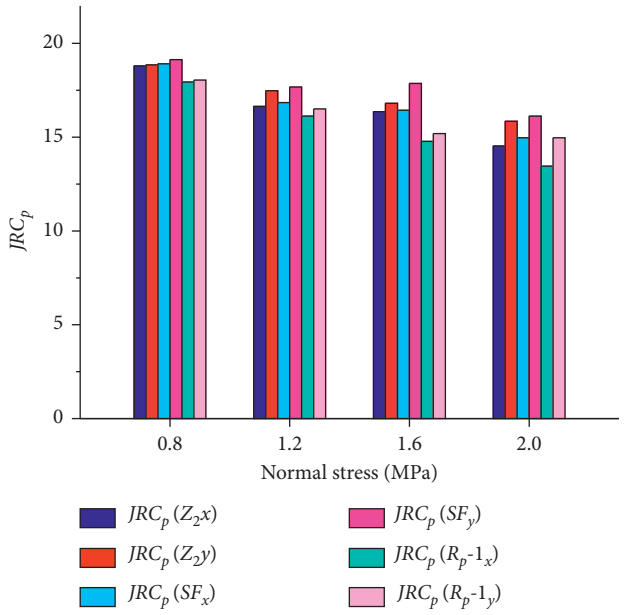

Figure 11: Comparison of JRC_p extracted profiles from the x and y directions.

perpendicular to the shearing direction (x direction) in Figure 8. The difference between the roughness statistical parameters and JRC_p along the two directions was investigated, which provides a basis for a reasonable determination of roughness and shear strength of joints. In this study, 10 profiles were extracted from the x and y directions of the shear surface in Figure 8. Spacing of 10 mm between two profiles was adopted, and the measuring point interval for each profile was 0.5 mm. The values of Z_2, SF, and R_p were determined with equations (1)–(3), as shown in Table 3. The roughness of each profile can be calculated with equations (4)–(6), and JRC_p of the joint surface can be obtained based on the roughness of profiles and equations (4)–(6).

JRC_p (Z_2), JRC_p (SF), and JRC_p ($R_p - 1$) calculated in x and y directions of four shear surfaces are plotted in Figure 11. Distinct differences exist between the values of JRC_p obtained via extracted profiles from x and y directions, which indicates the directional heterogeneity. JRC_p (Z_2), JRC_p (SF), and JRC_p ($R_p - 1$) obtained via extracted profiles in the y direction are slightly greater than those obtained via extracted profiles in the x direction. Such a phenomenon can be attributed to the influence of rotation and tension shear failure when shearing, which leads to greater roughness along the shear direction on the failure surface.

Meanwhile, Figure 11 illustrates that the values of JRC_p (Z_2), JRC_p (SF), and JRC_p ($R_p - 1$) decrease with the increase of normal stress in either direction. Specifically, JRC_p (Z_2) obtained via extracted profiles from the x direction is taken as an example for analysis. JRC_p (Z_2) gradually decreases when the normal stress increases from 0.8 MPa to 2.0 MPa, indicating that the joint surface becomes smoother. This owes to the shear failure and grind of the sawtooth with the increase of normal stress, resulting in the decrease of roughness and a smoother shear surface.

4. Conclusion

In regard of the difficulty in accurately determining the value of roughness of 3D joint, that is, the JRC, a new determination method, based on the 3D laser scanning technique and self-compiled Python code as well as the statistical parameter methods, was proposed in this study. The following conclusions are obtained:

(1) The joint was divided into several rectangular regions by roughness profiles, and the JRC of joint was assumed as the arithmetic average of the JRC of profiles, which overcomes the disadvantages of traditional 2D JRC determination methods and provides certain theoretical guidances for the calculation of 3D JRC.

(2) Equipped with the 3D laser scanning technique, the accurate 3D coordinate data of joint surface were easily obtained, and therefore, the data were processed via a self-compiled Python code, extracting the precise roughness profiles of the joint. The value of JRC of each roughness profile was calculated via the statistical parameter methods, where the statistical parameters Z_2, SF, and R_p were selected.

(3) The shear strength of jointed rock was evaluated via the JRC-JCS model, and therefore, a comprehensive comparison between the calculating results and experimental results was executed, which presents an excellent consistency of shear strength between the calculating values and experimental results, verifying the validity and accuracy of the proposed method.

(4) The influencing factors of roughness profile extraction on the accuracy of the JRC, such as measuring point interval, the profile number and direction, were investigated. A smaller measuring point interval can produce a more accurate digital profile. To a certain extent, the more the numbers of profiles, the smaller the value of JRC. The profile number of 10 was suggested in this study. Finally, the determination of JRC is directional, resulting in different values in the parallel and perpendicular direction of shearing.

Data Availability

The data used to support the findings of this study are available from the corresponding author upon request.

Conflicts of Interest

The authors declare no conflicts of interest.

Acknowledgments

This study gets its funding from project (51774322) supported by National Natural Science Foundation of China, Hunan Provincial Key Research and Development Program (2022SK2082), and project (2018JJ2500) supported by Hunan Provincial Natural Science Foundation of China. The authors wish to acknowledge these supports.

References

[1] Y. Shen, Y. Wang, Y. Yang, Q. Sun, T. Luo, and H. Zhang, "Influence of surface roughness and hydrophilicity on bonding strength of concrete-rock interface," *Construction and Building Materials*, vol. 213, pp. 156–166, 2019.

[2] Y.-J. Shen, G.-S. Yang, H.-W. Huang, T.-L. Rong, and H.-L. Jia, "The impact of environmental temperature change on the interior temperature of quasi-sandstone in cold region: experiment and numerical simulation," *Engineering Geology*, vol. 239, pp. 241–253, 2018.

[3] X. Fan, P. H. S. W. Kulatilake, and X. Chen, "Mechanical behavior of rock-like jointed blocks with multi-non-persistent joints under uniaxial loading: a particle mechanics approach," *Engineering Geology*, vol. 190, pp. 17–32, 2015.

[4] H. Lin, Y. Zhu, J. Yang, and Z. Wen, "Anchor stress and deformation of the bolted joint under shearing," *Advances in Civil Engineering*, vol. 2020, Article ID 3696489, 10 pages, 2020.

[5] Y. Zhao, L. Zhang, W. Wang et al., "Creep behavior of intact and cracked limestone under multi-level loading and unloading cycles," *Rock Mechanics and Rock Engineering*, vol. 50, pp. 1–16, 2017.

[6] Ö. Satıcı and B. Ünver, "Assessment of tunnel portal stability at jointed rock mass: a comparative case study," *Computers and Geotechnics*, vol. 64, pp. 72–82, 2015.

[7] H. Lin, X. Zhang, Y. Wang et al., "Improved nonlinear Nishihara shear creep model with variable parameters for rock-like materials," *Advances in Civil Engineering*, vol. 2020, Article ID 7302141, 15 pages, 2020.

[8] H. Lin, X. Zhang, R. Cao, and Z. Wen, "Improved nonlinear burgers shear creep model based on the time-dependent shear strength for rock," *Environmental Earth Sciences*, vol. 79, no. 6, p. 149, 2020.

[9] G. Zhang, M. Karakus, H. Tang, Y. Ge, and L. Zhang, "A new method estimating the 2D joint roughness coefficient for discontinuity surfaces in rock masses," *International Journal of Rock Mechanics and Mining Sciences*, vol. 72, pp. 191–198, 2014.

[10] C.-C. Xia, Z.-C. Tang, W.-M. Xiao, and Y.-L. Song, "New peak shear strength criterion of rock joints based on quantified surface description," *Rock Mechanics and Rock Engineering*, vol. 47, no. 2, pp. 387–400, 2014.

[11] P. S. Andrade and A. A. Saraiva, "Estimating the joint roughness coefficient of discontinuities found in metamorphic rocks," *Bulletin of Engineering Geology and the Environment*, vol. 67, no. 3, pp. 425–434, 2008.

[12] Z. C. Tang and L. N. Y. Wong, "New criterion for evaluating the peak shear strength of rock joints under different contact states," *Rock Mechanics and Rock Engineering*, vol. 49, no. 4, pp. 1191–1199, 2016.

[13] J. Shen, M. Karakus, and C. Xu, "Direct expressions for linearization of shear strength envelopes given by the generalized Hoek-Brown criterion using genetic programming," *Computers and Geotechnics*, vol. 44, pp. 139–146, 2012.

[14] N. Barton and V. Choubey, "The shear strength of rock joints in theory and practice," *Rock Mechanics*, vol. 10, no. 1-2, pp. 1–54, 1977.

[15] R. Tse and D. M. Cruden, "Estimating joint roughness coefficients," *International Journal of Rock Mechanics and Mining Science & Geomechanics Abstracts*, vol. 16, no. 5, pp. 303–307, 1979.

[16] M. Wang, P. Cao, and Y. Chen, "Anisotropy of rock profile JRC values and its empirical formula: a case study on yellow rust granite," *Geotechnical & Geological Engineering*, vol. 35, no. 4, pp. 1645–1655, 2017.

[17] M. Sanei, L. Faramarzi, S. Goli, A. Fahimifar, A. Rahmati, and A. Mehinrad, "Development of a new equation for joint roughness coefficient (JRC) with fractal dimension: a case study of bakhtiary dam site in Iran," *Arabian Journal of Geosciences*, vol. 8, no. 1, pp. 465–475, 2015.

[18] E. S. Gadelmawla, M. M. Koura, T. M. A. Maksoud, I. M. Elewa, and H. H. Soliman, "Roughness parameters," *Journal of Materials Processing Technology*, vol. 123, no. 1, pp. 133–145, 2002.

[19] Y. Li and Y. Zhang, "Quantitative estimation of joint roughness coefficient using statistical parameters," *International Journal of Rock Mechanics and Mining Sciences*, vol. 77, pp. 27–35, 2015.

[20] G. M. Yu, H. P. Xie, and J. A. Wang, "Fractal geometry of geological fracture," *Journal of China Coal Society*, vol. 21, pp. 459–463, 1996.

[21] H. Q. Sun and H. P. Xie, "Fractal interpolated surface and its dimensional theorem," *Journal of China University of Mining & Technology*, vol. 27, pp. 217–220, 1998.

[22] H. P. Xie, "Fractal description of rock joints," *Chinese Journal of Geotechnical Engineering*, vol. 17, pp. 18–23, 1995.

[23] P. Alameda-Hernández, J. Jiménez-Perálvarez, J. A. Palenzuela et al., "Improvement of the JRC calculation using different parameters obtained through a new survey method applied to rock discontinuities," *Rock Mechanics and Rock Engineering*, vol. 47, no. 6, pp. 2047–2060, 2014.

[24] R. Yong, X. Fu, M. Huang, Q. Liang, and S.-G. Du, "A rapid field measurement method for the determination of joint roughness coefficient of large rock joint surfaces," *KSCE Journal of Civil Engineering*, vol. 22, no. 1, pp. 101–109, 2018.

[25] Y. Zhao, L. Zhang, J. Liao, W. Wang, Q. Liu, and L. Tang, "Experimental study of fracture toughness and subcritical crack growth of three rocks under different environments," *International Journal of Geomechanics*, vol. 20, Article ID 04020128, 2020.

[26] B. S. A. Tatone and G. Grasselli, "A new 2D discontinuity roughness parameter and its correlation with JRC," *International Journal of Rock Mechanics and Mining Sciences*, vol. 47, no. 8, pp. 1391–1400, 2010.

[27] S. Du, "A new technique for fast measurement of JRC," *Journal of Engineering Geology*, vol. 10, pp. 98–102, 2002.

[28] G. Grasselli and P. Egger, "Constitutive law for the shear strength of rock joints based on three-dimensional surface parameters," *International Journal of Rock Mechanics and Mining Sciences*, vol. 40, no. 1, pp. 25–40, 2003.

[29] Y.-H. Lee, J. R. Carr, D. J. Barr, and C. J. Haas, "The fractal dimension as a measure of the roughness of rock discontinuity profiles," *International Journal of Rock Mechanics and Mining Science & Geomechanics Abstracts*, vol. 27, no. 6, pp. 453–464, 1990.

[30] M. Askari and M. Ahmadi, "Failure process after peak strength of artificial joints by fractal dimension," *Geotechnical & Geological Engineering*, vol. 25, no. 6, pp. 631–637, 2007.

[31] G. Zhang, M. Karakus, H. Tang, Y. Ge, and Q. Jiang, "Estimation of joint roughness coefficient from three-dimensional discontinuity surface," *Rock Mechanics and Rock Engineering*, vol. 50, pp. 1–12, 2017.

[32] C. Wang, L. Wang, and M. Karakus, "A new spectral analysis method for determining the joint roughness coefficient of rock joints," *International Journal of Rock Mechanics and Mining Sciences*, vol. 113, pp. 72–82, 2019.

[33] K. Li, Y. Cheng, Z.-Y. Yin, D. Han, and J. Meng, "Size effects in a transversely isotropic rock under brazilian tests: laboratory testing," *Rock Mechanics and Rock Engineering*, vol. 53, no. 6, pp. 2623–2642, 2020.

[34] D. Han, K. Li, and J. Meng, "Evolution of nonlinear elasticity and crack damage of rock joint under cyclic tension," *International Journal of Rock Mechanics and Mining Sciences*, vol. 128, Article ID 104286, 2020.

[35] K. Zhang, P. Cao, G. Ma, W. Wang, W. Fan, and K. Li, "Strength, fragmentation and fractal properties of mixed flaws," *Acta Geotechnica*, vol. 11, no. 4, pp. 901–912, 2016.

[36] R. Yong, J. Ye, B. Li, and S.-G. Du, "Determining the maximum sampling interval in rock joint roughness measurements using Fourier series," *International Journal of Rock Mechanics and Mining Sciences*, vol. 101, pp. 78–88, 2018.

[37] Y. Zhao, C. Zhang, Y. Wang, and H. Lin, "Shear-related roughness classification and strength model of natural rock joint based on fuzzy comprehensive evaluation," *International Journal of Rock Mechanics and Mining Sciences*, vol. 137, Article ID 104550, 2021.

[38] S. M. El-Soudani, "Profilometric analysis of fractures," *Metallography*, vol. 11, no. 3, pp. 247–336, 1978.

[39] H.-S. Jang, S.-S. Kang, and B.-A. Jang, "Determination of joint roughness coefficients using roughness parameters," *Rock*

Mechanics and Rock Engineering, vol. 47, no. 6, pp. 2061–2073, 2014.

[40] C. C. Xia and Z. Q. Sun, *Engineering Rock Joint Mechanics*, Tongji Press, Shanghai, China, 2002.

[41] Y. Wei, L. Jiaxin, L. Zonghong, W. Wei, and S. Xiaoyun, "A strength reduction method based on the generalized Hoek-Brown (GHB) criterion for rock slope stability analysis," *Computers and Geotechnics*, vol. 117, Article ID 103240, 2020.

[42] W. Wang, W. Yuan, X. Li, and B. Bai, "Evaluation approach of the slope stability based on deformation analysis," *International Journal of Geomechanics*, vol. 16, Article ID 04015054, 2016.

[43] W.-c. Fan, P. Cao, and L. Long, "Degradation of joint surface morphology, shear behavior and closure characteristics during cyclic loading," *Journal of Central South University*, vol. 25, no. 3, pp. 653–661, 2018.